SEISMOTECTONICS

EARTH SCIENCES
RESEARCH JOURNAL

Earth Sci. Res. J. Vol. 19, No. 2 (December, 2015): 121 - 127

UNIVERSIDAD
NACIONAL
DE COLOMBIA
SEDE BOGOTÁ
FACULTAD DE CIENCIAS
DEPARTAMENTO DE GEOCIENCIAS
RESEARCH GROUP IN GEOPHYSICS

Strain Rate Analysis on the Çankiri-Bingöl Segment of the North Anatolian Fault in Turkey

Hakan Yavasoglu
Istanbul Technical University
Insaat Fakultesi, Geomatik Muhendisligi Bolumu,
Maslak, Istanbul, 34469, Turkey
yavasoglu@itu.edu.tr

ABSTRACT

The North Anatolian Fault Zone (NAFZ) is one of the most important fault zones of Turkey and the world. It has produced several high magnitude earthquakes that have resulted in massive loss of lives and resources. National and international research on the North Anatolian Fault zone that Turkey resides on have been realized to better understand and predict the earthquakes produced by it. This study focuses on the Çankırı – Bingöl segment of the NAFZ. The aim of this study is to calculate the strain and latent earthquake potential of the studied area. For this purpose, geodetic data coming from several individual projects have been merged. Strain values have been calculated from the combined data and regions on the fault zone, and strain accumulations have been presented graphically. After calculation, Çankırı, Amasya and Kelkit regions were analyzed. The compressional and extensional deformation has been shown in north and south part of Çankırı basin, respectively. Eastern adjacent area of the Çankırı basin, Amasya region, has the primary branch of the NAF and its subbranches. In the Amasya region, the deformation is mostly on the main branch and the earthquake potential has risen to it. The Kelkit Valley has complex structures and inhomogeneous dispersion. Southeastern and Northwestern part of the Kelkit Valley has varied deformation in micro scale. Consequently, the study results indicate that strain accumulation is concentrated on areas such as the Çankırı basin, Amasya region, and various areas in the Kelkit Valley from west to east.

Keywords: GPS, Strain Rate, Earthquake, Deformation, Geodynamics.

Análisis de la Velocidad de Deformación en el Segmento Çankırı-Bingöl de la Falla de Anatolia del Norte, Turquía

RESUMEN

La Zona de la Falla de Anatolia del Norte (NAFZ, del inglés North Anatolian Fault Zone) es una de las zonas de fallas más importantes de Turquía y del mundo. Esta falla ha generado varios terremotos de gran magnitud que han resultado en pérdidas humanas y de recursos. La investigación nacional e internacional de la Zona de la Falla de Anatolia del Norte, que atraviesa Turquía, se ha realizado con el fin de un mejor entendimiento y predicción de los terremotos que allí se originan. Este análisis se enfoca en el segmento Çankırı-Bingöl de la NAFZ. El objetivo es calcular la tensión y el potencial de terremoto del área de estudio. Con este propósito se recopiló la información geodésica de varios proyectos individuales. Los valores de tensión se calcularon de la información combinada de las regiones que componen la zona de falla y se presentan gráficamente las acumulaciones de tensión. Tras el cálculo de estos valores se analizaron las regiones Çankırı, Amasya y Kelkit. La deformación de compresión y la de extensión aparecen al norte y al sur de la cuenca Çankırı, respectivamente. El área ubicada al Este de la cuenca Çankırı, la región de Amasya, posee la rama principal de la NAFZ y sus subdivisiones. En la región de Amasya la deformación se presenta en la rama principal de la NAFZ, donde se eleva el potencial de movimientos sísmicos. El valle de Kelkit tiene estructuras complejas y dispersión no homogénea. El sudeste y el noroeste del valle Kelkit muestran una deformación variada a microescala. Los resultados de este estudio indican que la acumulación de tensión se concentra en la cuenca Çankırı, la región Amasya y varias áreas del valle Kelkit desde el oeste hacia el este.

Palabras clave: GPS, velocidad de deformación, terremoto, deformación, geodinámica.

Record
Manuscript received: 11/02/2015
Accepted for publication: 28/07/2015

How to cite item
Yavasoglu, H. (2015). Strain rate analysis on the Çankırı-Bingöl segment of the North Anatolian fault in Turkey. *Earth Sciences Research Journal, 19(2)*, 121-127.
http://dx.doi.org/10.15446/esrj.v19n2.49063

INTRODUCTION

The NAFZ is one of the most offensive fault system all over the world and approximately 1500km long strike-slip fault system delineating the boundary between Eurasia and Anatolia plates (Barka and Kadinsky-Cade, 1988). The NAFZ runs along the northern part of Turkey, from Karliova in the east to the Gulf of Saros in the west and connects the East Anatolian compressional regime to the Aegean extensional regime.

The study area is bordered by the coast of the Black Sea in the north, Çankırı – Ilgaz (Kastamonu) in the west, the Sungurlu residential area in the south and Bingöl – Karlıova in the east. The main and secondary branches of the North Anatolian Fault have meant that the study area has been dissected into several continental blocks (Fig 1).

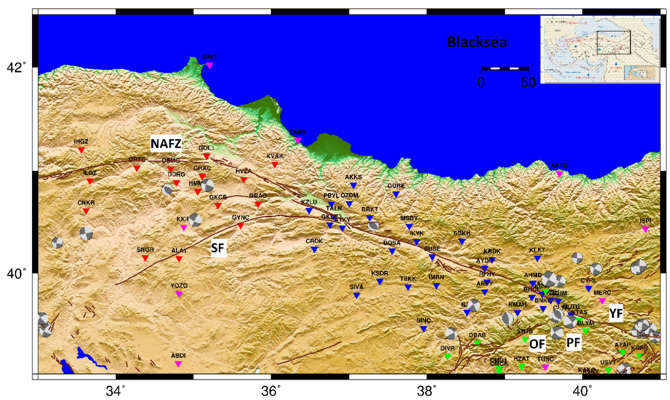

Figure 1. Reverse triangles are GPS sites, reds from Yavasoglu et al., 2011, blues from Tatar et al., 2012, greens from Ozener et al., 2010 and magentas from Reilinger et al. 2006. The tectonic map of study area, NAFZ-North Anatolian Fault Zone, SF-Sungurlu (Ezinepazar) Fault, OF-Ovacık Fault, PF-Pülümür Fault and YF-Yedisu Fault. The focal mechanism of earthquakes (beach balls) were obtained from globalcmt web page.

According to recent research (İşseven and Tüysüz, 2006; Kozacı et al., 2007; Tatar et al., 2012), the continental blocks that are bordered by faults move independently in different directions around a vertical axis. Also, it is important to understand how the potential energy of deformation accumulates and releases regarding spatial and time variables. Space-based geodetic technology enables us to determine the degree of crustal deformation with millimeter accuracy. So, it is possible to estimate present-day tectonic strain accumulation on the NAFZ using these geodetic technologies and fault mechanism incorporating variables such as slip rates, locking depths, fault geometry, etc. (Straub et al., 1997; Armijo et al., 1999; McClusky et al., 2000; Reilinger et al. 2006; Ozener et al. 2010; Yavasoglu et al. 2011; Tatar et al. 2012; Peyret et al., 2013).

Since 1990 many pieces of research have been undertaken in the area. These were mostly on a micro scale geodetic network or a global scale, but with an inadequate density of geodetic stations (McClusky et al., 2000; Hubert-Ferrari et al., 2002; Hartleb et al., 2003; Reilinger et al. 2006; and Kozacı et al., 2007). Velocity field derivatives from an inadequate density of networks affect the results. Additionally, in micro-scale studies, tectonic activity bordering the surveyed area cannot be distinguished sufficiently. Therefore, an analysis incorporating both a large scale study (covering all the area) and adequate localization resolution is needed.

In this study, the aim is to combine previous micro-scale geodetic studies and an estimate of the earthquake potential of the region using strain analysis computation (Write et al., 2001; Reilinger et al., 2006, Ozener et al. 2010; Yavasoglu et al. 2011; Tatar et al. 2012). The variations of the slip/strain rate and deformations in the study areas were investigated through a rigorous combination of the published micro scale geodetic data as a primary and new contribution.

Moreover, with this study, the NAFZ segment located between longitudes E33 and E41 degrees was investigated. There are three sub-segments in this area. The first section runs from Kastamonu to Amasya, the second segment from Amasya to Erzincan, and the last part from Erzincan to Bingöl. Historical and instrumental records indicate that they are active (Ambraseys, 1970, 2009; Barka, 1992, 1996; Barka et al., 2000). Another important aspect of this region is the fault behavior. What are the general characteristics of tectonic loading in this region? This is the main question concerning how loading is accommodated by the NAFZ. To answer these issues, firstly the tectonic and the seismic settings of the study area are summarized, and then the combined GPS velocity field is presented, and finally, the model results obtained from GPS velocities are discussed.

TECTONIC SETTINGS

The North Anatolian Fault Zone (NAFZ) which is the best-known dextral strike-slip faults in the world because of its remarkable seismic activity, separates the Anatolian plate from the Eurasia plate. The Anatolia plate escapes to the West about the Eurasia plate along the NAFZ. The NAFZ system has a strike-slip and right lateral tectonic settings because of two important mechanisms: The first is the Arabian plate push it in the East, and the second, it escape to the west along the Hellenic arc. (McClusky et al., 2000; Bozkurt, 2001; Sengor et al., 2004; Bayrak et al., 2009 and 2011).

In the 20th Century, many destructive earthquakes happened on the NAFZ, affecting the lives of millions and causing damage regarding billions of dollars in the study area (Table 1). Besides the 1999 earthquakes affecting Izmit and Düzce, most of the destructive earthquakes happened on the central and east segments, from Kastamonu to Bingöl (Table 1, Tan et al., 2008).

Table 1. Major earthquakes of last century in the area. (URL1)

Date	Latitude (°)	Longitude (°)	Depth	Magnitude
14.03.2005	39.354	40.890	5.0	5.8
12.03.2005	39.440	40.978	11	5.6
27.01.2003	39.5	39.85	16.1	6
27.01.2003	39.503	39.851	16.1	6
06.06.2000	40.73	33	7	6
06.06.2000	40.737	33.005	7	6
13.03.1992	39.718	39.622	25.9	6.7
28.03.1954	39.1	41	-	6.8
13.08.1951	40.8	33.4	-	6.5
17.08.1949	39.5	40.6	-	6.6
01.02.1944	40.844	33.292	35	7.2
26.11.1943	40.912	33.392	25	7.5
20.12.1942	40.671	36.45	35	7.2
26.12.1939	39.77	39.533	35	7.7
19.04.1938	39.439	34.015	35	6.6
24.01.1916	41	37	-	7.2
09.02.1909	40	38	60	6.6

The NAFZ extends to the Karlıova (Bingöl) triple junction in the East and the Aegean Sea in the west. It formed about 13 to 11 Ma in the east and propagated westward at about 11 cm/yr according to geological studies (Sengor et al., 2004). However, the NAFZ was formed in early Pliocene according to several scientist like Barka and Kadinsky-Cade, (1988) and Bozkurt (2001). The segmentation of the NAF and the structure of its splines are still in conflict. According to Sengor et al., (2004), The NAFZ bounds the Anatolian plate to the north. Its width, which is about 100 km, steadily increases from east to west, even though some pinched or swollen zones exist and the fault is located along an interface that separates subduction-accretion material to the south, from the older and stiffer continental basement to the north.

The NAFZ has been known to incorporate a uniform and homogenous structure in many segments. However, present day GPS data and strain analysis show us that it is not strictly uniform and homogenous from east to west. Many studies prove that the geological settings are different for each segment (Bozkurt, 2001; Sengor et al., 2004; Bayrak et al., 2009 and 2011; Peyret et al., 2013). Therefore, the velocity and seismicity of each segment of the NAFZ is also different.

In this area, the type of deformation is strike-slip along the fault. On the other hand, the central part of the NAFZ fault deformation has a standard component, because the fault is parallel to the Black Sea coastline. Additionally, geological evidence indicates compressive strain near the Ilgaz Mountains (Piper et al., 2010). The main offsets on the NAFZ are in the Pontide suture which is located close to the city of Erzincan (longitude E39◦20') (Sengor et al., 1985), around the Sea of Marmara (Armijo et al., 1999), and in the western part of the central bend (Hubert-Ferrari et al., 2002). The cumulative displacement of the NAFZ is about 80 km as has been indicated by evidence obtained from river deflection such as appertain to the Yeşilırmak, Kızılırmak and Gerede rivers (Hubert-Ferrari et al., 2002; Sengor et al., 2004; Peyret et al., 2013). Moreover, previously estimated geological slip rates of ±18 mm/yr (Hubert-Ferrari et al., 2002) to ±20.5 mm/yr (Kozacı et al., 2007) are in consensus with present day GPS derivative slip rates as determinated by block modeling that ranges from 17 to 25 mm/yr (McClusky et al., 2000; Reilinger et al., 2006; Yavasoglu et al., 2011).

The aim of the earth science studies on the NAFZ is to understand the large-scale behavior of the NAFZ zone. For this purpose, geodetic networks have been established on the NAFZ segments (McClusky et al., 2000; Reilinger et al., 2006; Ozener et al., 2010; Yavasoglu et al., 2011; Tatar et al., 2012).

In this study, the horizontal GPS velocity fields published by Reilinger et al. (2006), Ozener et al. (2010), Yavasoglu et al. (2011) and Tatar et al. (2012) will be used as a reference. These velocities have been estimated from at least 3 GPS campaigns and have been computed by using geodetic GPS process software such as GAMIT/GLOBK and BERNESE. Therefore, the velocities are accurate to the sub-millimeter level.

GEODETIC STUDIES

Today, InSAR (Synthetic Aperture Radar Interferometry) and GPS (Global Positioning System) are the most common methods used to observe tectonic movements. During the last decades, applications of such usage have been expanded, and precision of calculation has been increased. In this research, GPS data that has been gathered from research published between 2006 and 2012, have been included in the analysis.

Geodetic studies have been carried out concerning local regions. Although global scale measurements have been performed in previous studies (McClusky et al., 2000; and Reilinger et al., 2006), their cover area does not represent the entire fault zone, and the number of geodetic points was limited. Therefore, it is once more expressed that geodetic studies should be merged and analyzed accordingly (Table 2).

Table 2. GPS sites velocities used in strain rate computation.

Long (°)	Lat (°)	E&N Rate mm/yr		E&N 1-Sigma uncertainties (mm/year)		RHO	Sites	Reference
41.057	38.959	-9.32	14.57	0.66	0.64	-0.075	SOLH	Ozener et al., (2010)
40.733	39.182	-15.71	4.73	1.67	2.13	-0.062	KRPR	
40.575	38.758	-4.95	17.14	0.71	0.69	-0.131	GENC	
40.515	39.215	-18	5.35	1.62	2.13	-0.076	ATAP	
40.33	39.039	-20.2	7.9	1.96	2.58	-0.101	USVT	
40.105	38.949	-17.33	6.23	0.62	0.67	-0.043	KLKY	
40.052	38.963	-17.33	6.23	0.62	0.67	-0.043	KAKO	
40.038	39.43	-13.31	8.51	3.25	4.24	-0.05 3	BLYM	
39.957	39.538	-12.76	2.89	1.52	1.88	-0.075	KTAS	
39.91	38.737	-18.76	11.13	0.61	0.59	-0.072	SRYB	
39.524	39.824	-7.36	-1.39	1.18	1.47	-0.053	KCMZ	
39.258	39.35	-19.25	4.12	1.28	1.59	-0.051	SRTS	
39.217	39.074	-20.63	12.1	1.5	1.86	-0.069	HZAT	
38.931	39.026	-19.06	12.58	0.83	0.98	-0.089	CMGK	
38.922	39.059	-19.06	12.58	0.83	0.98	-0.089	CMG1	
38.645	39.31	-21.9	9.77	1.37	1.67	-0.085	DBAS	
38.264	39.178	-17.01	12.9	1.34	1.59	-0.104	DIVR	
Long (°)	Lat (°)	E&N Rate mm/yr		E&N 1-Sigma uncertainties (mm/year)		RHO	Sites	Reference
36.046	41.065	-4.46	4.94	1.34	1.64	-0.086	KVAK	Yavasoglu et al., (2011)
35.83	40.681	-14.9	7.64	1.01	1.22	-0.057	GBAG	
35.645	40.919	-11.97	7.37	1.17	1.38	-0.093	HVZA	
35.604	40.471	-21.2	2.96	1.2	1.47	-0.163	GYNC	
35.316	40.666	-16.16	5.9	1.21	1.49	-0.03	GKCB	
35.166	41.146	-8.69	5.19	1.19	1.51	-0.118	GOL1	
35.113	40.949	-14.5	6.34	1.24	1.44	-0.091	GHAC	
35.054	40.802	-15.56	5.3	0.93	1.14	-0.074	HMMZ	
34.814	40.145	-20.38	3.99	1.07	1.25	-0.065	ALA1	
34.78	40.888	-16.26	2.49	0.65	0.54	-0.145	DDRG	
34.707	41.022	-12.75	4.71	0.66	0.52	-0.121	OSMC	
34.379	40.155	-22.25	3.97	0.67	0.64	-0.047	SNGR	
34.272	41.031	-13.72	3.35	1.34	1.6	-0.074	ORTC	
33.668	40.905	-18.87	2.04	3.74	1.82	-0.232	ILGZ	
33.62	40.614	-21.03	2.97	1.07	1.11	-0.089	CNKR	
33.558	41.208	-3.34	1.43	0.62	0.6	-0.025	IHGZ	
Long (°)	Lat (°)	E&N Rate mm/yr		E&N 1-Sigma uncertainties (mm/year)		RHO	Sites	Reference
33.102	29.141	-1.09	6.75	0.69	0.65	0.006	ABOZ	Reilinger et al., (2006)
33.191	37.378	-13.63	2.53	0.6	0.59	0.005	MELE	
33.228	28.163	-2.01	7.14	0.66	0.65	0.005	GARB	
33.391	27.919	-1.92	7.22	0.65	0.64	0.002	ZEIT	
33.396	35.141	-6.24	3.11	0.53	0.53	0	NICO	
33.404	28.631	-2.93	4.98	0.65	0.64	0.004	DERB	
33.494	27.686	-1.69	5.07	0.65	0.64	0	GEMS	
33.596	28.269	-3.18	6.29	0.58	0.57	0.004	TOUR	
33.832	27.244	-3.36	5.82	0.82	0.77	-0.003	HURG	
33.883	27.961	-4.61	8.74	1.01	1.01	-0.008	KENS	
33.991	44.413	0.02	1.06	0.66	0.66	0.001	CRAO	
33.995	28.639	-0.87	6.38	1.03	1.04	-0.011	CATH	
34.184	27.846	-3.4	7.25	0.58	0.57	0.001	SHAM	
34.256	36.566	-11.59	4.94	0.69	0.69	0	MERS	
34.314	28.178	-2.17	8.06	0.87	0.8	-0.003	NABQ	
34.47	28.529	-3.05	7.42	0.63	0.63	0.001	DAHA	
34.552	36.9	-12.2	4.37	1.08	0.96	0.029	MER0	
34.763	30.598	0.47	8.64	0.55	0.55	0	RAMO	
34.781	32.068	-1.73	7.46	0.51	0.51	-0.001	TELA	
34.803	39.106	-19.36	3.89	1.5	1.49	-0.025	ABDI	
34.813	39.801	-18.84	5.38	0.66	0.64	0.005	YOZG	
34.866	31.378	-2.97	7.7	0.74	0.74	0	LHAV	
34.875	40.453	-17.6	4.78	0.94	0.91	-0.016	KKIR	
34.921	29.509	-0.45	8.86	0.53	0.53	0	ELAT	
35.023	32.779	-3.53	8.57	0.49	0.49	0	BSHM	
35.089	31.723	-1.61	7.28	1.18	1.12	-0.012	BARG	
35.145	33.023	-3.78	8.18	0.57	0.57	0	KABR	
35.202	31.771	-2.86	8.59	0.95	0.93	0.005	JSLM	
35.205	42.02	-0.56	1.72	0.87	0.77	0.007	SINO	
35.392	31.593	-2.32	8.9	0.64	0.63	0.001	DRAG	
35.416	32.479	-3.58	9.66	0.57	0.57	0	GILB	
35.674	34.115	-6.87	8.39	0.95	0.95	0	LAUG	
35.688	32.995	-1.68	11.97	0.52	0.52	-0.002	KATZ	
35.771	33.182	-2.68	11.26	0.66	0.66	0	ELRO	
35.87	36.397	-5.41	9.51	1.7	1.62	-0.001	ULCN	
35.94	36.456	-9.6	9.71	1.04	1	0.003	ULUC	
36.1	29.139	1.57	12.55	0.87	0.85	0.001	HALY	
36.131	36.05	-5.12	10.2	0.65	0.63	-0.015	SENK	
36.18	36.54	-9.89	12.17	1.73	1.75	-0.033	ISKE	
36.245	38.231	-13.82	8.39	1.59	1.44	-0.016	PNLR	
36.285	33.51	-2.27	11.9	0.95	0.95	-0.001	UDMC	
36.33	37.572	-14.11	8.91	1.66	1.6	-0.031	ANDR	
36.336	41.299	0.29	2.77	0.98	0.99	0.049	SAMS	
36.378	26.458	3.24	14.09	1.77	1.77	-0.002	ALWJ	
36.465	36.531	-7.41	11.86	0.9	0.82	0.007	ABAK	
36.524	36.788	-7.8	10.13	0.67	0.67	-0.004	HASA	
36.57	55.115	1.51	-0.04	1.2	1.18	-0.005	MOBN	
36.643	37.088	-7.45	10.98	0.76	0.72	-0.016	FEVZ	
36.758	55.699	0.59	-1.1	0.45	0.45	-0.005	ZWE2	
36.759	55.699	0.59	-1.1	0.45	0.45	-0.005	ZWEN	
36.972	37.19	-8.18	11.63	0.49	0.5	-0.009	SAKZ	
36.996	37.522	-9.38	10.6	0.55	0.57	-0.02	KMAR	
37.106	36.685	-7.95	10.53	1.77	1.74	-0.06	KILI	
37.113	37.747	-11.97	8.31	0.69	0.68	-0.011	ABEY	
37.22	38.179	-13.24	9.37	0.66	0.67	-0.017	ELBI	
37.224	56.027	0.32	0.8	0.58	0.57	0.001	MDVO	
37.436	37.518	-7.4	11.49	0.68	0.7	-0.014	ALAR	
37.574	36.901	-6.73	13.7	0.56	0.53	-0.012	GAZI	

Long (°)	Lat (°)	E&N Rate mm/yr		E&N 1-Sigma uncertainties (mm/year)		RHO	Sites	Reference
37.869	38.05	-13.34	9.73	0.68	0.67	-0.014	ALTP	Reilinger et al., (2006)
37.886	37.541	-7.1	12.58	0.74	0.73	-0.011	CKRH	
37.902	37.237	-6.82	13.61	0.68	0.68	-0.021	ARGA	
38.049	44.552	-0.16	-1.02	1.5	1.32	-0.024	GELE	
38.215	38.456	-11.48	10.92	0.74	0.72	-0.012	MLT1	
38.231	37.747	-7.57	14.06	0.83	0.8	-0.002	ADYI	
38.584	9.081	1.04	6.68	0.99	0.78	-0.01	KOLO	
38.766	9.035	1.03	6.53	0.51	0.44	-0.003	ADD0	
39.242	44.704	-0.22	0.05	1.27	1.13	0.018	GKL_	
39.254	38.64	-13.64	10.88	1.24	1.2	-0.046	GMKV	
39.282	8.472	3.29	6.34	0.63	0.54	0.012	BOKU	
39.438	8.292	4.1	6.03	0.7	0.55	0.03	SELA	
39.52	8.258	4.38	5.54	0.57	0.51	-0.005	BOLO	
39.524	39.071	-16.97	11.96	1.45	1.3	-0.004	TUNC	
39.531	8.266	4.38	5.54	0.57	0.51	-0.005	REDG	
39.631	21.369	7.59	15.54	1.79	1.78	-0.001	JEDD	
39.702	40.974	0.68	2.55	0.47	0.45	0.009	AKTO	
39.805	37.847	-8.91	15.11	0.75	0.74	-0.006	KRCD	
40.194	-2.996	2.85	5.23	0.52	0.5	0	MALI	
40.254	39.731	-2.81	5.81	0.75	0.68	-0.015	MERC	
40.272	43.681	1.83	-1.09	1.68	1.41	0.006	KRPO	
40.65	37.246	-6.44	16.64	0.8	0.75	-0.023	KIZ2	
40.809	40.437	0.72	3.31	0.56	0.51	-0.015	ISPI	
41.3	39.973	-0.66	5.88	0.66	0.64	0.008	ERZU	
41.339	41.371	-0.54	2.83	0.9	0.89	-0.017	HOPA	Reilinger et al., (2006)
41.454	39.186	-5.88	10.74	2.01	1.29	-0.046	VART	
41.512	39.643	-2.09	4.39	1.78	1.22	-0.072	TKMN	
41.565	43.788	0.78	1.23	0.44	0.43	0.004	ZECK	
41.565	43.788	0.78	1.23	0.44	0.43	0.004	ZELB	
41.794	38.754	-4.69	14.76	0.84	0.69	0.107	KRKT	
41.99	40.548	1.95	5.07	0.93	0.9	0.02	OLTU	
Long (°)	**Lat (°)**	**E&N Rate mm/yr**		**E&N 1-Sigma uncertainties (mm/year)**		**RHO**	**Sites**	**Reference**
40.079	39.852	−5.71	2.73	0.52	0.65	−0.086	CYRL	Tatar et al., (2012)
39.853	39.591	−13.11	8.17	0.54	0.67	−0.089	MUTU	
39.725	39.582	−12.19	9.56	0.54	0.67	−0.084	CLYN	
39.688	39.724	−11.36	3.56	0.54	0.67	−0.083	UZUM	
39.593	39.733	−10.52	3.37	0.57	0.73	−0.098	EKSU	
39.494	39.652	−15.59	5.35	0.82	1.07	−0.055	BNKC	
39.482	39.793	−10.52	0.77	0.52	0.64	−0.083	ER98	
39.42	40.151	−4.55	1.6	0.27	0.26	−0.034	KLKT	
39.361	39.902	−4.24	−1.26	0.52	0.64	−0.090	AHMD	
39.349	39.762	−13.57	3.37	0.61	0.77	−0.078	BHCL	
39.164	39.613	−10.87	7.71	0.47	0.57	−0.088	KMAH	
38.836	40.136	−4.09	2.7	0.49	0.61	−0.092	KRDK	
38.774	39.914	−13.87	5.92	0.44	0.54	−0.081	RFHY	
38.743	39.82	−18.39	9.6	0.45	0.53	−0.082	ARPY	
38.743	40.047	−10.58	0.12	0.51	0.64	−0.088	AYDG	
38.515	39.614	−11.76	8.02	0.48	0.58	−0.092	ILIC	
38.448	40.316	−5.05	−1.70	0.46	0.55	−0.087	SBKH	
38.121	39.882	−13.35	7.48	0.55	0.69	−0.108	IMRN	
38.067	40.162	−14.74	7.03	0.55	0.68	−0.102	SUSE	
37.958	39.454	−18.18	9.88	0.5	0.58	−0.068	SINC	
37.869	40.313	−7.74	4.87	0.45	0.53	−0.082	IKYK	
37.771	40.463	−4.46	4.98	0.46	0.54	−0.067	MSDY	
37.757	39.867	−18.82	10.13	0.46	0.56	−0.101	TEKK	
37.604	40.778	−2.12	1.41	0.26	0.24	−0.027	GURE	
37.549	40.221	−17.47	7.73	0.41	0.48	−0.085	DOSA	
37.394	39.921	−21.28	5.96	0.45	0.54	−0.090	KSDR	
37.265	40.547	−9.09	5.18	0.41	0.48	−0.090	BRKT	
37.095	39.786	−20.33	8.58	0.26	0.24	−0.035	SIVA	
37.054	40.863	−1.13	−0.85	0.43	0.53	−0.104	AKKS	
37.001	40.685	−5.48	4.07	0.45	0.55	−0.088	OZDM	
36.912	40.447	−19.95	6.09	0.97	1.28	−0.088	ATKY	
36.804	40.557	−13.52	5.23	0.48	0.57	−0.103	TALN	
36.77	40.68	−5.77	3.12	0.41	0.48	−0.090	PBYL	
36.752	40.476	−14.42	6.74	0.45	0.54	−0.097	GKDE	
36.554	40.237	−20.73	7.08	0.25	0.23	−0.032	CRDK	
36.485	40.617	−17.18	4.8	0.39	0.46	−0.095	KZLU	

STRAIN RATE CALCULATION (MODELING)

The GPS data obtained from different projects (papers) have been transformed into the same datum. Then, the Eurasia fixed velocity field has been calculated. The data used in this study have been processed using geodetic software GAMIT/GLOBK, which can to provide velocity vectors with sub-millimeter accuracy.

The velocity field is necessary to show the movement of Anatolian Plate. But it is usually not sufficient for earth science purposes. Velocity field data gathered from GPS data is meaningful when translated into strain and slip values using block modeling or elastic half-space modeling.

The general approach associated with this method is to obtain a continuous strain field via a different interpolation of the east and north velocity components (Wessel and Bercovici, 1998) on a regular grid using the splines in tension algorithm using only geodetic data. A factor (T) controls the tension. T=0 is the minimum curvature, and T=1 is the maximum curvature. Also, the GPS sites must be sufficiently distributed to cover all the area under consideration, and they must be distributed in such a way as to cover an area bigger than the grid size. It was tested the T values and set to T=0.3 as recommended by Hackl et al. (2009). The area was divided into cells using the grid size. They contain more than one observation. The median of all the included data was computed for each, with the regions having a large number of comments in need of being averaged. In this way, outliers and bias can be removed.

The interpolation will give two continuous scalar fields from east and north velocities are independent for the interseismic period. In this way, the spline interpolation function can be applied to calculate the strain rate tensor for two components of the velocity fields.

The elements of the strain rate tensor are defined in Hackl et al. (2009) as;

$$\dot{\varepsilon}_{ij} = \frac{1}{2}\left(\frac{\partial v_i}{\partial x_j} + \frac{\partial v_j}{\partial x_i}\right) \qquad (1)$$

Where i, j substitute east and north.

In a similar way, it is possible to compute the antisymmetric rotation rate tensor:

$$\dot{\omega}_{ij} = \frac{1}{2}\left(\frac{\partial v_i}{\partial x_j} - \frac{\partial v_j}{\partial x_i}\right) \qquad (2)$$

At this point, any tensorial analysis can be performed.

The eigenspace analysis of the tensor is the starting point for the full description of deformation at every grid point, providing different aspects of the strain rate. The eigenvectors of the strain rate, for example, represent the direction of maximum and minimum strain rates, while their associated real eigenvalues λ1 and λ2 represent the magnitude (note that the notation that positive values indicate extension and negative values stand for compression was followed) (Hackl et al., 2009).

The maximum shear strain rate and its direction might provide a tool to identify active faults since motion along faults is related to shear on that structure. Faults oriented in this direction are the ones most likely to rupture in a seismic event. The maximum shear strain rate at every grid point can be obtained by a linear combination of the maximum and minimum eigenvalues:

$$\dot{\varepsilon}_{\max\_shear} = \frac{\lambda_1 - \lambda_2}{2} \qquad (3)$$

While the direction of maximum shear is oriented 45◦ from the direction of the eigenvector corresponding to the largest eigenvalue:

$$\theta_{1,2} = \frac{1}{2}\arctan\left(\frac{2\dot{\varepsilon}_{ij}}{\dot{\varepsilon}_{ii} - \dot{\varepsilon}_{jj}}\right) \pm 45° \qquad (4)$$

Note that Eq. (4) corresponds to two conjugate perpendicular directions that cannot be distinguished without further constraint.

The trace of the tensor,

$$\delta = \dot{\varepsilon}_{ii} + \dot{\varepsilon}_{jj} \qquad (5)$$

Corresponds to the relative variation rate of surface area (dilatation) and thus can indicate regions of thrusting or normal faulting (Hackl et al., 2009).

Therefore, strain rates, the variation rate of the area under consideration, maximum and minimum share and strain rate tensor were calculated from the velocity field obtained from GPS data using a method published in Hackl et al. (2009) in detail, (Figs. 2, 3).

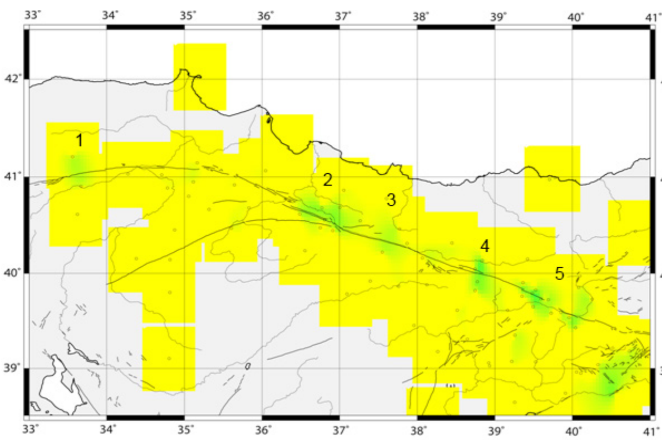

Figure 2. The map represents strain rate distribution, green regions are the most active areas, the numbers (1, 2, 3, 4, 5) are shown Çankırı, Amasya, Kelkit, Erzincan and Karlıova regions, respectively.

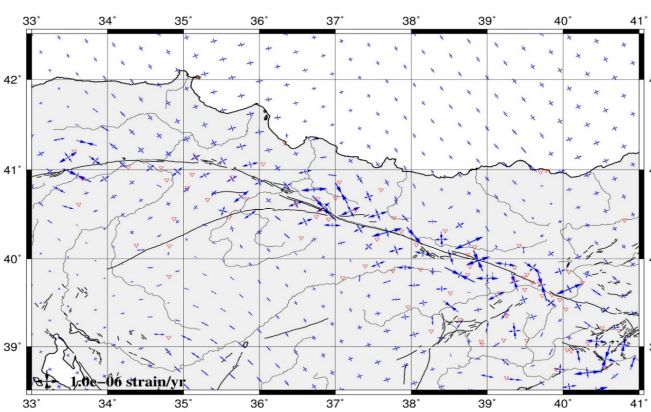

Figure 3. The map represents strain rate distribution, red reverse triangles are the location of the GPS sites.

Based on the allocation of the GPS observations, different grid sizes were tested to identify the best resolution. The ideal situation would be to have a grid with at least one observation per cell. After various tests, it was found that a regular grid with a cell size of 0.03◦ is most suitable for the interpolation of the horizontal velocity field components for this region. Using GMT routines (Wessel and Smith, 1998), the strain rate tensor was calculated. Figures 2, 3 shows the three components of the strain rate tensor. This method is more suitable to determine relative strain and strain rate changes (Hackl et al., 2009).

The plate boundary along the NAFZ is mainly of strike-slip nature. Thus, the direction and magnitude of the maximum shear strain rate are good scalar fields to represent the strain rate tensor. These two parameters are suitable to characterize the amount of localization of the shear deformation and the direction along which strike-slip faulting is more favorable. In Figures 2, 3, the color scale indicates the magnitude of the maximum shear strain rate, while the crosses indicate the two conjugate maximum shear directions. The maximum shear strain rate is highest in the southeast (Region-4 and 5) along the NAFZ (max 0.44 µstrain/yr) and along the central section of the NAFZ (Region-2 and 3) (max 0.33 µstrain/yr). This matter can partially be a consequence of the fact that in these regions, the deformation can better localize along the major segments of the fault especially Region-2 and 3. The maximum shear strain rate is less in Region-1 according to the other four regions, but it has significant values (max 0.28 µstrain/yr) in Çankırı basin.

DISCUSSION

Biryol et al. (2010) suggest that comparison of fast polarization directions with plate motion directions requires selection of a reference frame that will yield true absolute plate velocities. There exist multiple reference frames for plate motions, based on different assumptions, and each of these has different motion directions and speeds. One of the most commonly used reference frames for our study area regards Eurasia as fixed and focuses on the relative motions of the surrounding plates (i.e. Anatolia) on fixed Eurasia (McClusky et al. 2000). In this case, the direction of lithospheric motion depends strictly on the selection of the fixed plate (i.e. Eurasia) and does not necessarily represent an absolute plate motion that can be used for comparison with mantle anisotropy measurements.

Regional strain rates for Anatolia indicate variations in the principal compressional and extensional strain axes from east to west, following the pattern of the counter-clockwise rotation of the Anatolian plate. This variation in direction for maximum compression and extension is also in agreement with the structural features of the Anatolian crust (Biryol et al., 2010).

Regarding the results of this study, there is a high degree of consistency between the results obtained with geodetic methods and geological–geophysical methods (Biryol et al., 2010). Therefore, the data used in this study, the modeling calculations, and the computed strain rates can be accepted. The study of regional strain rates is crucial for any seismic hazard assessment.

In this study, the velocity fields of the middle and eastern parts of the NAFZ have been merged to calculate the strain accumulation in a greater area. Similar studies have been realized previously in local areas. However, none of them either covered the focus area of this research nor were as large in scope. A previous study by McClusky et al. (2000) and Reilinger et al. (2006) should be noted, however, since they cover the same area of focus but with limited geodetic data.

The Çankırı basin (Region-1) that is located in different tectonic regimes is an active seismic region (Kaymakci et al., 2003; Yavasoglu et al., 2011; and Peyret et al., 2013). The strain accumulation in the Çankırı basin has been discussed in Kaymakci et al. (2003) and Peyret et al. (2013) concerning the possibility that it is a post-seismic strain that occurred after the Duzce (1999) earthquake, and the effects were thought to be improbable regarding the post-seismic activity. However, strain accumulation in Region-1 can be seen to be associated with a right lateral slip rate (Fig. 3). In this study, for the Çankırı basin, the northern side of the Çankırı basin indicates compressional deformation, and the southern side indicates extensional deformation. Besides, the rotational displacement is also shown (Cinku et al., 2011).

In Amasya (Region-2), the NAFZ exhibits a horse tail structure with the main branch and several secondary branches that extend into Anatolia. The most important and well-known of these branches is the Sungurlu (Ezinepazar) fault, on which deformation signs were not detected in this study, in concordance with Yavasoglu et al. (2011). However, it is known that the 1939 Erzincan earthquake also fractured the Sungurlu fault (İşseven and Tüysüz, 2006). Despite this, there is a concentrated strain accumulation in Region-2, where the Sungurlu fault and the NAFZ main branch merge. Between the main branch and the Sungurlu fault, a structure of normal and reverse faults have triggered the extension. Due to this extension, the strain has built up in the northern parts of the Region-2, and the earthquake potential has risen accordingly.

Kelkit Valley (Region-3) and Erzincan (Region-4) exhibit a very active setting. Seismicity is noteworthy in this region as is reported in Tatar et al. (2012). While Region-4 shows signs of compression, Region-3 shows signs of extension. In Region-3, the NAFZ is wider (Sengor et al., 2004). The tension that builds up in Region-2 also affects Region-3, which in turn continues the extension.

Karlıova (Region-5) is a very complex zone (Barka et al., 1987; Sengor and Yılmaz, 1981). Many physical elements contribute to the deformation where the right lateral NAFZ and the left lateral East Anatolian Fault Zone

(EAFZ) merge. The earthquakes of March 12 and 14, 2005 in Karlıova (Table 1) were the results of an extended period of seismic inactivity. The seismic gap that lasted from the year 1784 has been ended to a degree in this region. However, strain accumulation in the area can be postulated to be still building up. This complex structure also affects the results of this study. The tension in Region-5 does not exhibit a homogeneous dispersion. The fault segments found in the Yedisu, Ovacık and Pülümür faults should be investigated separately.

CONCLUSION

GPS velocity field data has been modeled for the strain rates in middle and eastern parts of the NAFZ, using published GPS derivative data (Reilinger et al., 2006, Ozoner et al., 2010, Yavasoglu et al., 2011, Tatar et al., 2012) and the mathematical model published in Hackl et al. (2009).

The presence of earthquake potential and strain accumulation in 5 regions in the middle and eastern parts of the NAFZ (Figs. 2, 3) have been found in this study. With the help of this new modeling method, the results are free of ambiguity regarding parameters such as fault locking depth, fault geometry, and are calculated to show present day activity using only geodetic data.

Between Region-1 and Region-2, there is no significant strike-slip or dip-slip on the Sungurlu fault that is the spline of the NAFZ. The sudden decrease in strain accumulation from the east (the Kelkit Valley) to the west (south of the Çankırı basin) reveals that all the strain is sufficiently accommodated by the main branch of the NAFZ.

Region-5 indicates a high strike-slip rate. The last rupture in the Region-5 was approximately 250 years ago (Ambraseys, 1970). The accumulated slip deficit is about 3m, corresponding to an earthquake potential of between Mw 7 and 7.7.

There is great risk concerning the five regions focused on in this study. Extensive and detailed seismic records are needed to estimate earthquake times and magnitude. Also, micro-geodetical research in the region should be increased. Multi-disciplinary studies on both the global and the local scale should be increased, especially in the regions where the NAFZ shows a very complex structure.

ACKNOWLEDGEMENTS

I would like to thank M. Hackle, R. Malservisi and S. Widowinski for their GMT scripts. I am grateful to T. Aykan Kepekli, Huseyin A. Yavasoglu and Ali Goksenli for their comments. This paper has been supported by TUBITAK (2219 scholarship) and ITU. Maps and figures were drawn using GMT (Wessel and Smith, 1998).

REFERENCES

Ambraseys, N.N. (1970). Some characteristics of the North Anatolian Fault Zone. Tectonophysics, 9, 143–165.

Ambraseys, N.N. (2009). Earthquakes in the Eastern Mediterranean and Middle East: A Multidisciplinary Study of Seismicity up to 1900. Cambridge University Press, New York, pp. 512–515.

Armijo, R., Meyer, B., Hubert, A. and Barka, A. (1999). Westward propagation of the North Anatolian fault into the northern Aegean: timing and kinematics. Geology, 27, 267–270.

Barka, A. A., Toksoz, M. N., Gulen, L., Kadinsky-Cade, K. (1987). Segmentation, seismicity, and earthquake potential of the eastern part of the North Anatolian Fault Zone. Bulletin of the Earth Sciences Application and Research Center of Hacettepe University, 14, 337–352.

Barka, A. (1992). The North Anatolian fault zone. Annales Tectonicae (Special Issue), 6, 164–195.

Barka, A. (1996). Slip distribution along the North Anatolian fault associated with large earthquakes of the period 1939 to 1967. Bulletin of the Seismological Society of America, 86, 1238–1254.

Barka, A., Akyüz, H.S., Cohen, H.A. and Watchorn, F. (2000). Tectonic evolution of the Niksar and Tasova-Erbaa pull-apart basins, North Anatolian Fault Zone: their significance for the motion of the Anatolian block. Tectonophysics, 322, 243–264.

Bayrak, Y., Öztürk, S., Çınar, H., Kalafat, D., Tsapanos, T.M., Koravos, G.C. and Leventakis, G.A. (2009). Estimating earthquake hazard parameters from instrumental data for different regions in and around Turkey. Engineering Geology 05: 200-210.

Bayrak, Y., Çınar, H., and Bayrak, E. (2011). The North Anatolian Fault Zone: an Evaluation of Earthquake Hazard Parameters. In "New Frontiers in Tectonic Research: At The Midst of Plate Convergence", edited by Uri Schattner, Intech Open Access Publisher, Croatia, Chapter 10, p.269-288.

Biryol, C.B., Zandt, G., Beck, S.L., Ozacar, A.A., Adiyaman H.E. and Gans, C.R. (2010). Shear wave splitting along a nascent plate boundary: the North Anatolian Fault Zone. Geophysical Journal International, 181, 1201-1213.

Bozkurt, E. (2001). Neotectonics of Turkey- a Synthesis. Geodinamica Acta, 14, 3-30.

Cinku, M.C., Hisarli, Z.M., Heller, F., Orbay, N. and Ustaomer, T. (2011). Middle Eocene paleomagnetic data from the eastern Sakarya Zone and the central Pontides: Implications for the tectonic evolution of north central Anatolia. Tectonics, 30, 1-19.

Hackl, M., Malservisi, R., and Wdowinski, S. (2009). Strain rate patterns from dense GPS networks. Natural Hazards and Earth System Sciences, 9, 1177-1187, doi:10.5194/nhess-9-1177-2009.

Hartleb, R.D., Dolan, J.F., Akyüz, H.S and Yerli, B. (2003). A 2000 year-long paleoseismologic record of earthquakes along the central North Anatolian fault, from trenches at Alayurt, Turkey. Seismological Society of America Bulletin, 93, 1935–1954.

Hubert-Ferrari, A., Armijo, R., King, G., Meyer, B. and Barka, A.A. (2002). Morphology, displacement, and slip rates along the North Anatolian fault, Turkey. Journal of Geophysical Research, 107, B10, 2235, 9/1–9/33.

İşseven, T. and Tüysüz, O. (2006). Paleomagnetically defined rotations of fault-bounded continental blocks in the North Anatolian Shear Zone, North Central Anatolia. Journal of Asian Earth Sciences, 28, 469-479.

Kahle, H.-G., Cocard, M., Peter, Y., Geiger, A., Reilinger, R., Barka, A. and Veis, G. (2000). GPS-derived strain rate field within the boundary zones of the Eurasian, African, and Arabian Plates. Journal of Geophysical Research, 105, 23353–23370.

Kaymakci, N., White, S.H., Van Dijk, P.M. (2003). Kinematic and structural development of the Cankırı basin (Central Anatolia Turkey): a paleostress inversion study. Tectonophysics, 364, 85–113.

Kreemer, C., Haines, J., Holt, W. E., Blewitt, G. and Lavallee, D. (2000). On the determination of a global strain rate model. Earth, Planets and Space, 52, 765–770.

Kozacı, O., Dolan, J.F., Finkel R. and Hartleb, R. (2007). Late Holocene slip rate for the North Anatolian fault, Turkey, from cosmogenic 36Cl geochronology: Implications for the constancy of fault loading and strain release rates. Geology, 35, 867-870.

McCaffrey, R. (2002). Crustal block rotations and plate coupling. S. Stein, J.T. Freymueller (Eds.), Plate Boundary Zones: Geodynamics Series, vol. 30 American Geophysical Union, 101–122

McCaffrey, R. (2005). Block kinematics of the Pacific–North America plate boundary in the southwestern United States from inversion of GPS, seismological, and geologic data. Journal of Geophysical Research, 110, p. B07401.

McClusky, S., Balassanian, S., Barka, A., Demir, C., Ergintav, S., Georgiev, I., Gurkan. O., Hamburger, M., Hurst, K., Kahle, H., Kastens, K., Kekelidze, G., King, R., Kotzev, V., Lenk, O., Mahmoud, S., Mishin, A., Nadriya, M., Ouzounis, A., Paradissis, D., Peter, Y., Prilepin, M., Reilinger, R., Şanlı, I., Seeger, H., Tealeb, A., Toksöz, M.N. and Veis, G. (2000). Global Positioning System constraints on plate kinematics and dynamics in the eastern Mediterranean. Journal of Geophysical Research 105, 5695-5719.

Ozener, H., Arpat, E., Ergintav, S., Dogru, A., Çakmak, R., Turgut, B. and Doğan, U. (2010). Kinematics of the eastern part of the North Anatolian Fault Zone. Journal of Geodynamics 49, 141–150.

Peyret, M., Masson, F., Yavasoglu, H., Ergintav, S. and Reilinger, R. (2013). Present-day strain distribution across a segment of the central bend of the North Anatolian Fault Zone from a Persistent-Scatterers InSAR analysis of the ERS and Envisat archives. Geophysical Journal International, 192, 929-945, DOI: 10.1093/gji/ggs085

Piper, J.D.A., Gürsoy, H., Tatar, O., Beck, M.E., Rao, A., Koçbulut, F., and Mesci, B.L. (2010). Distributed neotectonic deformation in the Anatolides of Turkey: A palaeomagnetic analysis. Tectonophysics, 488, 1–4, 31-50, ISSN 0040-1951.

Reilinger, R., McClusky, S., Vernant, P., Lawrence, S., Ergintav, S., Çakmak, R., Özener, H., Kadirov, F., Guliev, I., Stepanyan, R., Nadariya, M., Hahubia, G., Mahmoud, S., Sakr, K., ArRajehi, A, Paradissis, D., Al-Aydrus, A., Prilepin, M., Guseva, T., Evren, E., Dmitrotsa, A., Filikov, S.V., Gomez, F., Al-Ghazzi, R. and Karam, G. (2006). GPS constraints on continental deformation in the Africa-Arabia, Eurasia continental collision zone and implications for the dynamics of plate interactions. Journal of Geophysical Research, 111, B05411.

Sengor, A.M.C. and Yilmaz, Y. (1981). Tethyan evolution of Turkey: a plate tectonic approach. Tectonophysics, 75, 181–241.

Sengör, A.M.C., Görür, N. and Saroglu, F. (1985). Strike-slip faulting and related basin formation in zones of tectonic escape: Turkey as a case study, in Strike-Slip Faulting and Basin Formation. Eds. Biddle, K.T. & Christie-Blick, N., Society of Economic Paleontolgists and Mineralgists, Special Publications, 37, 227– 267.

Sengör, A.M.C., Tüysüz, O., Imren, C., Sakinc, M., Eyidogan, H., Görür, N., Le Pichon, X. and Rangin, C. (2004). The North Anatolian fault: a new look. Annual Review of Earth and Planetary Sciences, 33, 1–75.

Straub, C., Kahle, H.G. and Schindler, C. (1997). GPS and geologic estimates of the tectonic activity in the Marmara Sea region, NW Anatolia. Journal of Geophysical Research, 102(B12), 27 587–27 601.

Tan, O., Tapırdamaz, C. and Yoruk, A. (2008). The Earthquake Catalogues for Turkey. Turkish Journal of Earth Sciences, 17, 405–418.

Tatar, O., Poyraz, F., Gursoy, H., Cakir, Z., Ergintav, S., Akpinar, Z., Kocbulut, F., Sezen, F., Turk, T., Hastaoglu, O., Polat, A., Mesci, B. L., Gursoy, O., Ayazli, E., Cakmak, R., Belgen, A. and Yavasoglu, H. (2012). Crustal deformation and kinematics of the eastern part of the North Anatolian fault zone (Turkey) from GPS measurements. Tectonophysics, 518–521, 55–62.

United States Geological Survey. The maps and lists show events which have been located by the USGS and contributing agencies within the last 30 days. http://earthquake.usgs.gov/earthquakes/map (last accesed March 2014).

Wessel, P. and Bercovici, D. (1998). Interpolation with Splines in Tension: A Green's Function Approach. Mathematical Geology, 30, 77–93.

Wessel, P. and Smith, W.H.F. (1998). New, improved version of the Generic Mapping Tools released. Eos Transactions American Geophysical Union (AGU), 79, 579.

Wright, T.J., Parsons, B.E. and Fielding, E.J. (2001). Measurement of interseismic strain accumulation across the North Anatolian Fault by satellite radar interferometry. Geophysical Research Letters, 28, 2117–2120.

Yavasoglu, H., Tari, E., Tüysüz, O., Cakir, Z. and Ergintav, S. (2011). Determining and modelling tectonic movements along the central part of the North Anatolian Fault (Turkey) using geodetic measurements. Journal of Geodynamics, 51, 339–343